Research Article

Size investigation of silicon nanoclusters deposited on HOPG using noncontact atomic force microscopy

Mümin Mehmet KOÇ[1,2,*]

[1]Advanced Materials Engineering, School of Engineering, University of Portsmouth, Portsmouth, United Kingdom
[2]Department of Physics, Faculty of Science and Literature, Kırklareli University, Kırklareli, Turkey

Abstract: The sizes of silicon nanoparticles produced using two different novel methods are investigated in this report. The method of production used to generate silicon oxide nanoparticles was achieved via gas aggregation codeposition with water on a cold target, and also via a liquid jet method. The nanoparticles were drop-cast on a highly oriented pyrolytic graphite (HOPG) substrate and assessed using ultrahigh vacuum atomic force microscopy (AFM). Noncontact constant force mode was used in the AFM investigations. The silicon nanoparticles produced using the gas aggregation and water codeposition method were found to be smaller than 2 nm. A degree of deviation in the measured sizes of the silicon nanoparticles in different layers was detected. The size deviation was attributed to surface–nanoparticle, surface–tip, and nanoparticle–tip interactions. Silicon nanoparticles produced in alcohol using the liquid jet method were also found to be smaller than 2 nm. The solvent used for the silicon nanoparticles was varied in our investigations. When water was used as a solvent, a size deviation for silicon nanoparticles in different layers was also observed.

Key words: Silicon nanoparticles, highly oriented pyrolytic graphite, atomic force microscopy, size analysis

1. Introduction

Nanoparticles have been researched in various fields of the natural sciences like physics, chemistry, and engineering in considerable depth; industry uses nanoparticles for various practical applications. The aim of scientific research into nanoscience is to understand, manipulate, and control the properties of nanoobjects ranging from a few angstroms (10^{-10} m) to a couple of hundred nanometers (10^{-9} m) [1]. The nanoobjects in this range are considered to be a special phase between isolated atomic and bulk materials.

Among these nanoobjects, nanoclusters are of particular importance. Nanoclusters can be defined as the aggregation of a group of atoms or molecules ranging from two atoms to a couple of hundred thousand atoms, which can consist of atoms of a single element or those from a combination of multiple elements. The 'special' phase to which atomic clusters belong shows distinct properties depending on the number of atoms they contain. In addition, the properties of the atomic clusters change dramatically upon altering their size, to the extent that even the addition or removal of a single atom can make a huge difference [2–7]. To be more specific, altering the cluster size changes the surface area-to-volume ratio; specific surface area-to-volume ratio clusters show distinct and frequently novel physical properties [1,8,9].

In the literature, many different kinds and types of clusters have been studied and reported on [10–12]. Most such nanoparticles have been found to be highly reactive and sensitive to their environment. In particular,

---

*Correspondence: muminmehmetkoc@hotmail.com

metal nanoparticles have been found to be hazardous and toxic within a biological environment [13–15]. Having a low toxicity, being biofriendly, and showing favorable fluorescence properties has given silicon nanoclusters an important place among other nanoparticles [16–18]. The low toxicity of silicon nanoparticles finds areas of application where reducing the toxicity of certain metal nanoparticles is desirable [19,20]. Considering these parameters, silicon nanoparticles have been used in biolabeling and as marking tools for medical diagnostics and therapy [21–23]. The interaction of the nanoparticles with liquids chemically alters their structure [24,25].

For practical and technological and thin film applications of clusters as building blocks for nanomaterials, it is vital to understand the behavior of clusters on surfaces. Such comprehension may lead to potential applications such as electronic devices, memory devices, printable electronics, or batteries [26–30]. Therefore, it is important to understand the size characteristics and surface nanoparticle interactions to be able to gain control over them. To date, the behavior, nucleation, and agglomeration processes of metallic nanoparticles have been reported in the literature [31,32]. In addition, thin film formation of metallic clusters was previously studied with scanning tunneling microscopy [31]. There are only a limited number of studies in the literature investigating silicon nanoparticles using atomic force microscopy (AFM) techniques. Here, in this study, we report on the size and surface properties and the clusters and tip interactions for silicon clusters produced with two new production methods, namely the codeposition of silicon nanoparticles with water on a cold target [33,34] and a liquid jet method [35]. The production method allowed our group to produce fluorescent and chemically stable silicon nanoclusters in water and alcoholic liquids. The fluorescence and chemical structure of the nanoparticles produced by this method were already the subject of detailed study [34]. Hence, a detailed size investigation of the nanoparticles reported in this work will fill the associated gap in the literature.

2. Materials and methods

2.1. Nanoparticle production

The nanoparticles studied in this research were prepared in liquid and were produced by using two different methods: gas aggregation liquid co-deposition, and liquid jet.

2.1.1. Gas aggregation liquid co-deposition method

Silicon nanoparticles were produced via the gas aggregation codeposition with water method in a special ultrahigh vacuum (UHV) system called 'slumps'. A DC magnetron sputtering system was used as the atom source. In the production, Ar gas was flowed into the production chamber to allow sputtering of silicon atoms from the DC magnetron target. Sputtered silicon atoms collide with each other as mediated by the Ar gas to produce nanoparticles. Production of nanoparticles with the help of Ar gas is referred to as gas aggregation. The nanoparticles thus produced are then directed onto a cold target. The target was cooled with liquid nitrogen, where water molecules were sprayed before and during silicon deposition. Depositing silicon nanoparticles and water molecules simultaneously on the target is referred to as the gas aggregation with water codeposition technique. When the nanoparticle deposition was completed, the valve to the target chamber was closed to isolate the target chamber from the production chamber. The target chamber was then vented with Ar gas. The ice matrix consisting of silicon nanoparticles and water molecules was left to melt; the silicon nanoparticle suspension thus produced was collected in a collection dish (see references [28,29] for details of the production method and the production system).

2.1.2. Liquid jet method

Silicon nanoparticles were produced by the liquid jet method under high vacuum conditions [36]. The system used a DC magnetron source as an atomic source. The atoms were sputtered using Ar gas. When the Ar gas is applied to the system, free sputtered atoms, which behave like an atomic gas, fill the production chamber. A liquid microjet squirts water into the atomic vapor produced by the DC magnetron sputter. Liquid is squirted from a liquid jet capillary that points towards a liquid nitrogen-cooled target. When the jet of liquid passes through the sputtered atoms, the liquid entrains some of the free atoms, which then agglomerate in the liquid to form silicon nanoclusters. The liquid jet then hits the liquid nitrogen-cooled target and freezes there. When the deposition was competed, the production chamber was vented with Ar gas. The frozen ice matrix was then heated to produce a liquid suspension of silicon nanoparticles [35].

2.2. Sample preparation and AFM measurement

The nanoparticles produced in the liquid were kept in glass vials. Before their deposition onto highly oriented pyrolytic graphite (HOPG), a clean surface needed to be prepared. Therefore, the top layer of the HOPG was cleaved with Sellotape. An aliquot of nanoparticle suspension solution of 3 μL was taken by micropipette and drop-cast onto the cleaned HOPG crystal, which was then transferred to the vacuum chamber of the AFM. The sample was maintained in this chamber for 12 h until UHV conditions were achieved, after which it was transferred to the analysis chamber.

AFM was undertaken with an Omicron UHV scanning tunneling microscope/atomic force microscope at room temperature. Noncontact constant force mode was used in the measurements. A silicon nitride MikroMasch tip designed for noncontact measurements with a 20-nm tip radius was used as the scanning tip. The nominal stiffness of the tip was 40 nm^{-1} and the resonance frequency was 307 kHz. The microscope was calibrated using single and double HOPG steps, which gave step heights of 0.35 nm and 0.70 nm. After completion of AFM investigation, the raw data were obtained from the AFM computer and processed using WSXM software [37].

3. Results and discussion

3.1. Size deviation of multilayer nanoparticles

Size deviation of multilayered silicon nanoparticles produced with the water codeposition of gas aggregation method is investigated in this section. The silicon nanoparticles were drop-cast onto the HOPG substrate and investigated via AFM. A detailed explanation of drop-cast method and AFM investigation is given in the Section 2. Figures 1a–1f show combined images of the four different zones obtained from AFM investigations. Each zone was investigated in detail and data belonging to each region are presented in Figures 2, 3, and 4. A chart was presented to summarize these data, as reported in Table 1. In zone 1, single- and double-layered silicon nanoparticle formations in a branched shape exist in low coverage. In region 2, a highly covered thick-layered nanoparticle film structure can be seen in single-layer formations. In region 3, a partially covered section of double-layered silicon nanoparticle film is illustrated. In section 4, single- and double-layered semicovered silicon nanoparticle film structures could be seen on the surface.

In region 1 of Figure 1, a semicovered nanoparticle film was observed with branch-shaped silicon nanoparticle structures. A height distribution across the region was taken and is presented in Figure 2. A multiple layered section in the region was marked in Figure 1a. Figure 1b shows a magnified section from region 1. A double-layered structure of nanoparticles can be seen by visual inspection. The faint region indicated by the
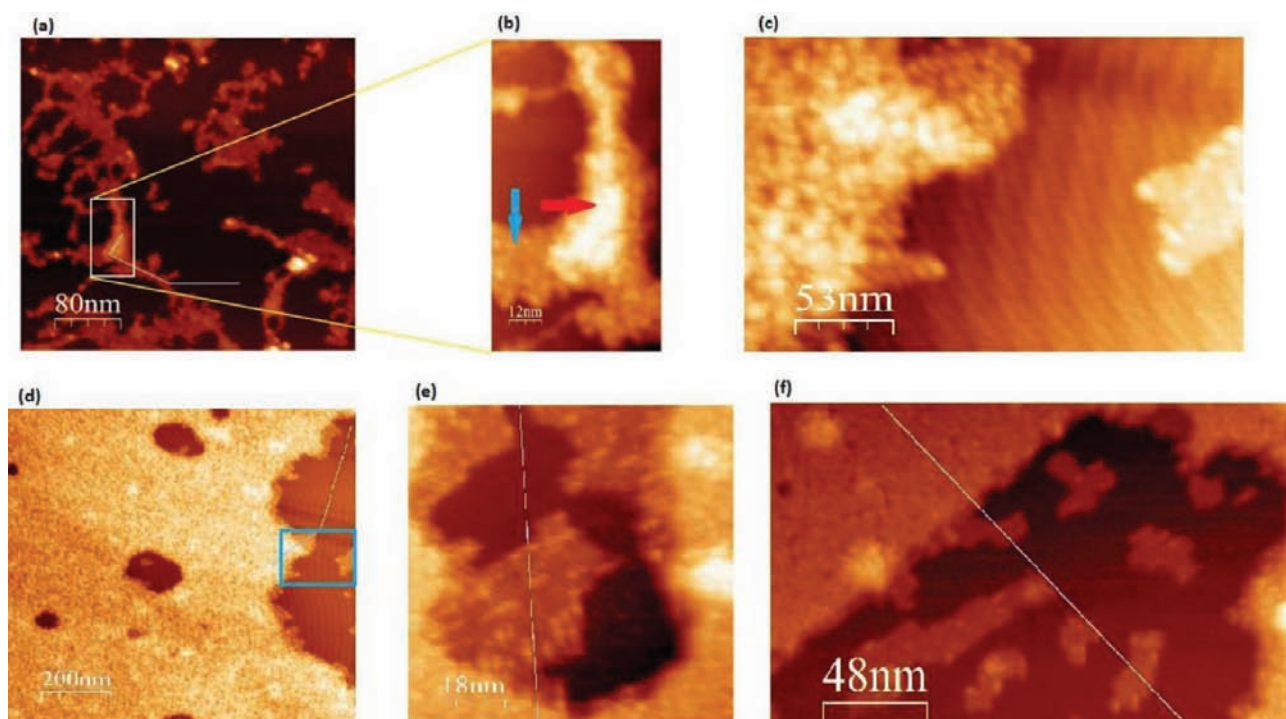
Figure 1. The AFM image of region 1 where the size measurements of the particles were performed. a) The whole of zone 1; the line shows where the height profile in Figure 2 was taken. b) An expansion of the region marked in (a). The blue arrow indicates the first layer and the red arrow indicates the second layer. c) An AFM image of an expansion of region of zone 2. d) An AFM image of zone 2. The line shows where the height profile in Figure 4b was taken. e) An AFM image of zone 3. The line shows where the height profile in Figure 4d was taken. f) An AFM image of zone 4. The line shows where the height profile in Figure 4f was taken.

Table 1. Table summarizing the important values found for baseline, first layer and second layer heights, and calculation of the cluster size in the first and second layers related to the height distributions and height profiles for zones 1, 2, 3, and 4. Si water codeposition; spec: special, gen: general.

Height distribution (HD) / height profile (HP)	Baseline (nm)	1st layer (nm)	2nd layer (nm)	Measured height in 1st layer (nm)	Measured height in 2nd layer (nm)
HD zone 1 (spec)	0.2	1	2.5	0.9 ± 0.1	1.4 ± 0.1
HD zone 1 (gen)	0.4	1.2		0.8 ± 0.1	
HP zone 1	0.2	1.2	2.6	1 ± 0.1	1.4 ± 0.1
HD zone 2	0.6	1.4	2.8	0.8 ± 0.1	1.4 ± 0.1
HP zone 2	0.4	1.2	2.7	0.8 ± 0.1	1.5 ± 0.15
HD zone 3	0.25	1.1	2.5	0.8 ± 0.05	1.4 ± 0.1
HP zone 3	0.2	1	2.4	0.8 ± 0.05	1.4 ± 0.1
HD zone 4	0.5	1.3	2.4	0.75 ± 0.1	1.1 ± 0.1
HP zone 4	0.4	1.2	2.4	0.8 ± 0.1	1.1 ± 0.1
Average				0.811 ± 0.07	1.35 ± 0.16

blue arrow in Figure 1 shows the first silicon nanoparticle layer, while the brighter region indicated by the red arrow shows the second silicon nanoparticle layer. The height distributions taken from Figures 1a and 1b are presented in Figure 2a and 2b, respectively. Both visual inspection and height distribution confirm the presence of a double-layered structure. The height profile and height profile investigations for zones 2 (Figure 1d), 3 (Figure 1e), and 4 (Figure 1f) are shown in Figure 4.
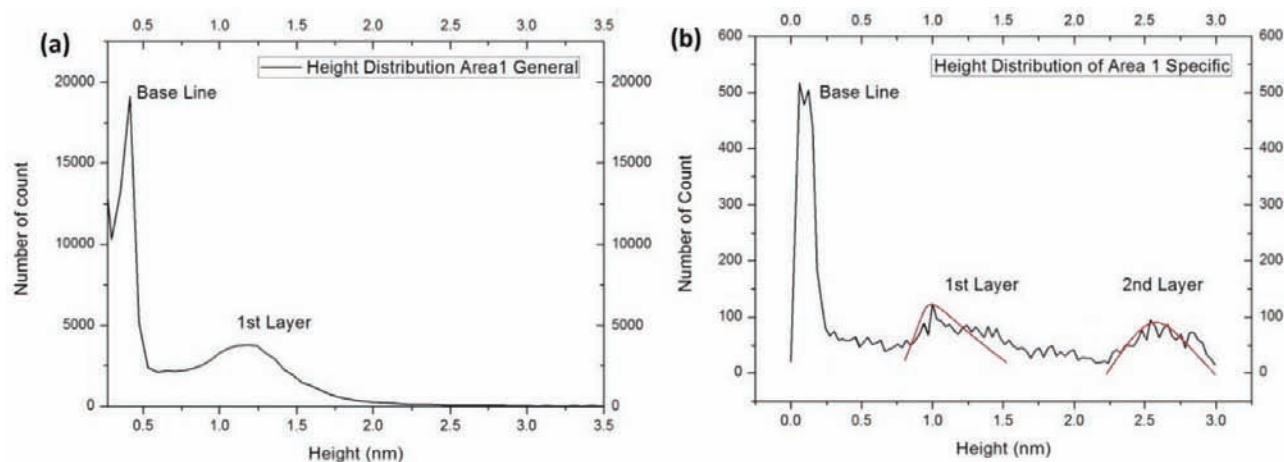

Figure 2. a) The height distribution of the AFM image in Figure 1a. b) The height distribution of the AFM image in Figure 1b; red dots are included to make visual inspection easier. Shift occurring due to the tilt can be seen in the graphs. The height distributions show the importance of the scale of the height distribution. Height distributions in small regions can give better resolution.

In Figure 2a, two distinct peaks can be seen. The first peak shows the base layer, which corresponds to the height of the HOPG substrate and tilt on the surface, and was found to be between 0.3 and 0.4 nm. The second peak observed at around 1.2 nm represents the height of a single layer of nanoparticles. The difference between the first layer peak and base layer gives a measure of the single nanoparticle height, which is 0.8 nm. Another distinct peak for the double- and triple-layered structures could not be observed in the height distribution illustrated in Figure 1a due to the high number of single-layered structures on the HOPG, whereas there was only a limited number of double- and triple-layered structures. Therefore, the single layer peak is very strong and the peaks for the second and third layers are faint over the whole measurement area. To be able to investigate the height of the single and double layers the region in Figure 1b was chosen. The height distribution obtained (see Figure 2b) from Figure 1b shows three distant peaks. The height of the base layer was found as 0.2 nm in these height measurements, where a relatively low tilt was obtained from a smaller area. The first layer peak was observed at 1 nm while the second layer peak was observed in the region of 2.5–2.6 nm. A height distribution investigation of the two different scales shows the importance of an appropriate assessment; reducing the region over which height distribution assessments were undertaken increased the associated accuracy. In the height distribution obtained from Figure 1b, the nanoparticle size measured for the first layer was found using the difference between the baseline peak and first layer peak, which was 0.9 ± 0.1 nm. The nanoparticle size on the second layer was found using the difference between the first layer and second layer peaks, which was around 1.4 ± 0.1 nm.

Beside the height distribution, a manual height profile analysis was also performed; the results of the height profile are presented in Figure 3. The height distribution was determined to compare the heights in two different aspects. The height distribution was used to evaluate the data using the mean height obtained

from the measured region, where the height profile shows the exact height of the cross-sectioned region where the height profile investigation was performed. It was expected that similar results would be seen for the two investigations.
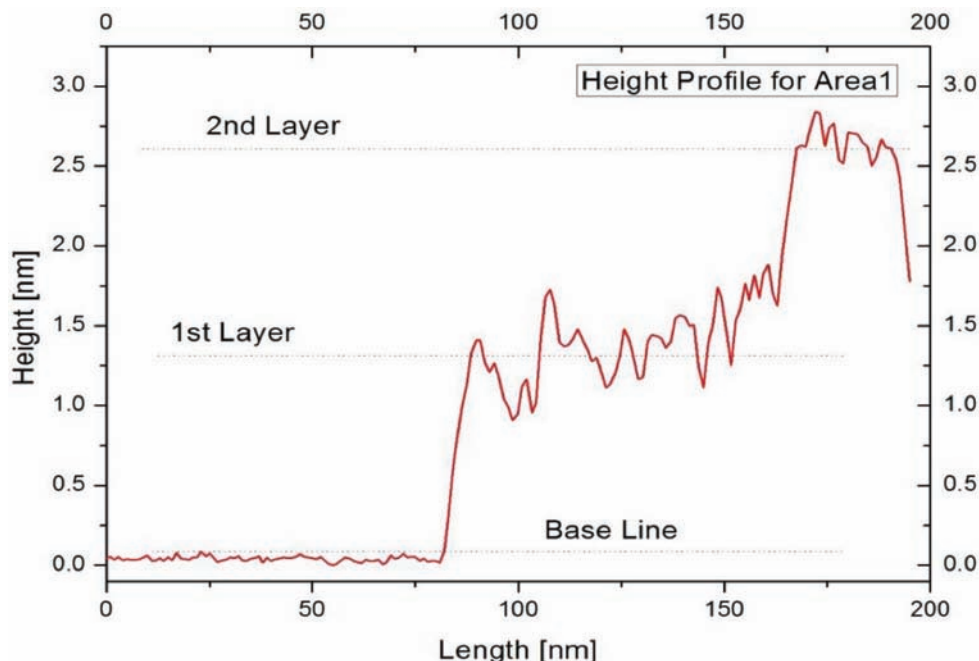

Figure 3. Height profile of the cross-sectional line in the AFM image in Figure 1a.

In the height profile investigation, the baseline was found to be about 0.15–0.20 nm. The height of the first layer was measured as about 1.25 nm and the height of the second layer was measured at around 2.60 nm. In this investigation, the nanoparticles in the first layer were measured at about 1.10 nm, while the nanoparticles in the second layer were measured at about 1.4 nm. In the height profile measurement, the height of the nanoparticles in the first layer seems to be a little larger than the nanoparticles measured using the height distribution. The nanoparticles in the second layers were found to be approximately the same via both techniques.

The height profile and height profile investigations for zones 2 (Figure 1d), 3 (Figure 1e), and 4 (Figure 1f) are shown in Figure 4. Baselines for the first and second layer heights were marked on the graphs and the nanoparticle heights obtained from each measurement are reported in Table 1.

The baseline peak in the height distribution corresponds to baseline layer in the height profile measurements. The baseline peak and baseline layer give the height of the surface that occurs due to the tilt or steps in the HOPG surface. The first layer peak in the height distribution corresponds to the first layer height in the height profile, while the second layer peak corresponds to the second layer height in the second layer. The height difference between the first layer and baseline gives the net measured nanoparticle size, where the height difference between the second and first layer gives the net measured nanoparticle size on the second layer.

The average heights of the nanoparticles measured in the first layer were found as 0.811 ± 0.070 nm in both the height distribution and height profile investigations, where the average heights of the nanoparticles in the second layer were found to be 1.35 ± 0.16 nm. A clear shift between the first and second layers was observed in our investigations (see Table 1 and Supplementary Table S1). Further results from the 20 height
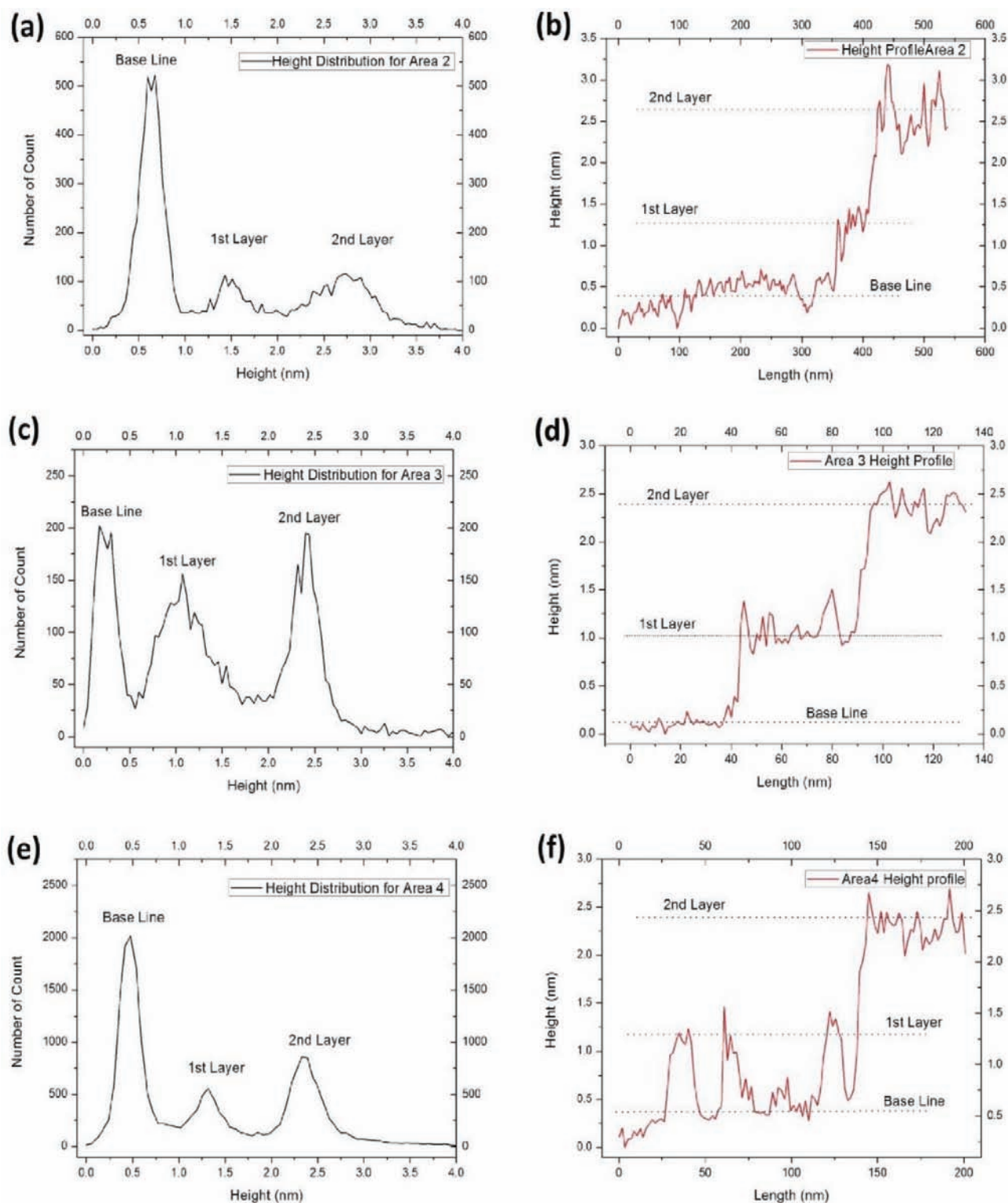
Figure 4. Height measurements and height profiles of zones 2, 3, and 4. a) Height distribution profile of zone 2 obtained from AFM images. b) Height profile measurement of zone 2 obtained from AFM images. c) Height distribution profile of zone 3 obtained from AFM images. d) Height profile measurement of zone 3 obtained from AFM images. e) Height distribution profile of zone 4 obtained from AFM images. f) Height profile measurement of zone 4 obtained from AFM images.

profile measurements conducted in total are presented in Table S1, where the average size of the nanoparticles in the first layer was found as 0.722 ± 0.086 nm and 1.58 ± 0.26 nm for the second layer. Hence, clear size shifts were evidenced by our measurements. A similar case was reported by Galinis et al. for silicon nanoparticles produced in a liquid medium [38]. Two possible scenarios were proposed to explain the nanoparticle size deviation: particle–particle, particle–surface attractions and particle–tip, surface–tip attractions.

The theory that deals with particle–particle, particle–surface interactions was proposed by Galinis et al. They believed that the attraction between the particles is less than the attraction that occurs between the particles and the surface. Therefore, they proposed a deformation of the cluster shape in the first layers that were directly interacting with the HOPG surface. They considered that in the second and third nanoparticle layers the attraction between the surface and the particles gradually decreased and the attraction between particles became dominant; hence, the size increased. However, the attraction between the AFM tip and the surface should also be considered. At this point, a second theory was offered to explain the deviation: particle–tip, surface–tip attraction.

The van der Waals energy becomes a driving force between nanoparticles and the nanoparticle–particle AFM tip. The van der Waals attraction energy was calculated using the following formula:

$$E = \frac{-HD}{24z},\tag{1}$$

where H is the Hamaker constant, $D = \frac{2D1D2}{D1+D2}$ is the reduced diameter, and z is the separation between the clusters. In noncontact mode, AFM obtains surface data by calculating the attraction between the tip and the surface. Table 2 shows the Hamaker constants between the materials used in the experiment. It can be seen that the Hamaker constant between the silicon nitride tip and carbon is larger than that between the silicon oxide nanoparticle and silicon nitride tip. Making measurements in single-layered clusters implies that the surface may be strongly affected by the tip, which may cause an apparent shift in the size of the nanoparticles in the first layer. In the measurement of the double- and triple-layered structures, no direct interaction between the tip and the surface occurs; hence, the effect of the substrate is significantly reduced, and the data obtained regarding the size of the nanoparticles can—at least apparently—be different for different layers.

Table 2. Hamaker constants of materials and some material combinations [39].

Material	Hamaker constant $[10^{-20}]$
Si_3N_4-Carbon	22
SiO_2-Carbon	13.7
Si_3N_4-SiO_2	12.1
SiO_2-SiO_2	7.2

3.2. Solvent effect on nanoparticle size

In this section, the size characteristics of the silicon nanoparticles produced by the liquid jet method will be evaluated. The motivation of this section is one of observing the change in silicon nanoparticle sizes for different solvents as an indication of the alteration of the resultant chemical and physical properties. In the previous section, the difference in sizes of the nanoparticles found in different nanoparticle layers was seen; in this section, a similar study was made for silicon nanoparticles produced using the liquid jet method.

The initial nanoparticles were produced in ethanol using the liquid jet method. To test the dependence of the size on the solvent used, different solvents were used to form nanoparticle suspensions. Three samples were taken from the original solution and placed in different vials. One of the samples was diluted with ethanol, as per the original sample, while the other two vials were left in the fume cupboard to dry. After the solvents had totally dried in the vials, one was topped up with isopropanol (IPA) and the other with pure water. Then the nanoparticles were drop-cast on the HOPG in the manner described in Section 2. While a large number of images were obtained from the measurements, just two images from each investigation are presented in this report.

The height information obtained from Figures 5a and 5b are presented in Figures 6a and 6b. In Figure 6a the height distribution obtained from Figure 5a is presented. The baseline peak was found to be about 0.5 nm. The first layer peak was seen at about 1.6 nm and the second layer peak was observed at 2.6 nm. The peak related to the third layer was seen at about 4 nm. The height profile obtained from Figure 5b is presented in Figure 6b. The data obtained from the height profile was found to be consistent with the data obtained from the height distribution. The threshold (baseline) in the height profile was found to be about 0.4 nm. The first layer was found at 1.5 nm, the second layer was found at 2.6 nm, and the third layer at 3.7 nm. In almost all layers the nanoparticle height was found to be about 1.1 nm, and, notably, no significant difference was seen in the heights from each layer. The case was confirmed by both height distribution and height profile assessments (see Table 3).
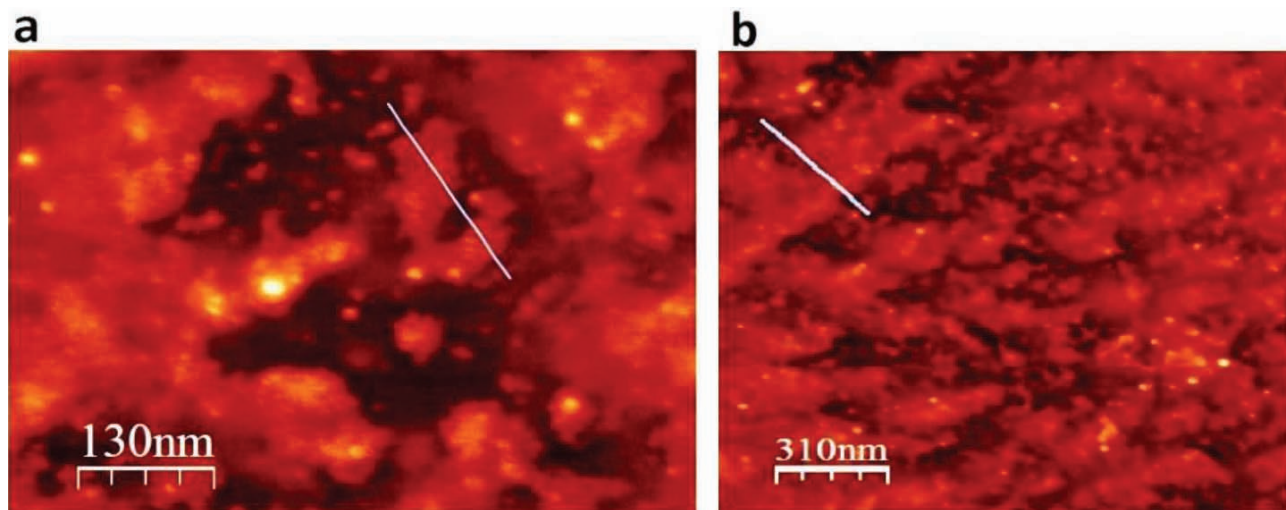

Figure 5. AFM images showing where the size measurement was performed. Images belong to the original sample diluted with ethanol. a) The blue line in the image shows where the height measurement was performed for a single-layered nanoisland. b) The blue line in the image shows where the height measurement was performed for a multilayered nanoisland.

AFM images of the silicon nanoparticles topped up with IPA are presented in Figure 7. Some of the large islands were spread around the surface, adopting various shapes, while some other islands adopted dot-like structures that can be easily identified in the images. These islands seemed to be formed in monolayer structures. The blue lines in the images indicate where the height profile measurements were performed. The results associated with the height profile measurement and height distribution are presented in Figure 7.

Height information obtained from Figures 7a and 7b are presented in Figures 8a and 8b, respectively.
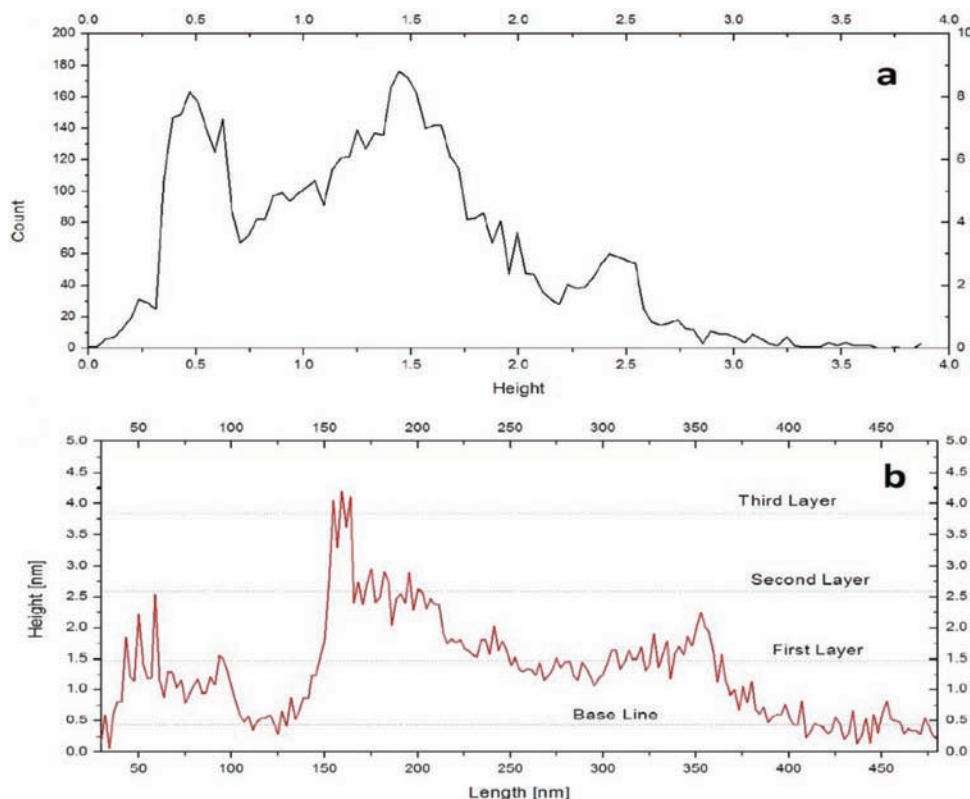
Figure 6. Graphs showing height profiles and height distributions for the images presented in Figure 5 (ethanol sample). a) Graph showing the height distribution of the multilayered island obtained from 5a. b) Graph showing the height profile of the blue line in Figure 5b.

Table 3. Size of nanoparticles in different solvents.

Sample type Height distribution (HD) / height profile (HP)	Baseline [nm]	First layer [nm]	Second layer [nm]	Third layer [nm]	Fourth layer [nm]	Size [nm]
Si in ethanol (HP)	0.2	1.2				1 ± 0.1
Si in ethanol (HP)	0.4	1.5	2.6	3.7		1.1 ± 0.15
Si in ethanol (HD)	0.5	1.6	2.6			1 ± 0.1
Si topped with IPA (HP)	0.3	1.1 ± 0.1				0.8 ± 0.1
Si topped with IPA (HD)	0.5	1.4				0.9 ± 0.5
Si topped with water (HP)	0.2	0.8	2	3.1	4.2	0.6 ± 0.1 / 1.1 ± 0.1
Si topped with water (HD)	0.4	2.2	3.5	4.8		1.1 ± 0.1

Figure 8a shows the height profile taken from Figure 7a, where the blue line was shown. The baseline in the height profile was measured at about 0.3 nm. The height taken from the top of the monolayer was found to be 1.2 nm, which gives an approximate particle size of 0.8–0.9 nm. The height distribution obtained from Figure 7b is presented in Figure 8b. The baseline peak in the height distribution graph was found at about 0.5 ± 0.05 nm, where the first layer peak was seen at 1.4 ± 0.05 nm. The nanoparticle size obtained from the graph was
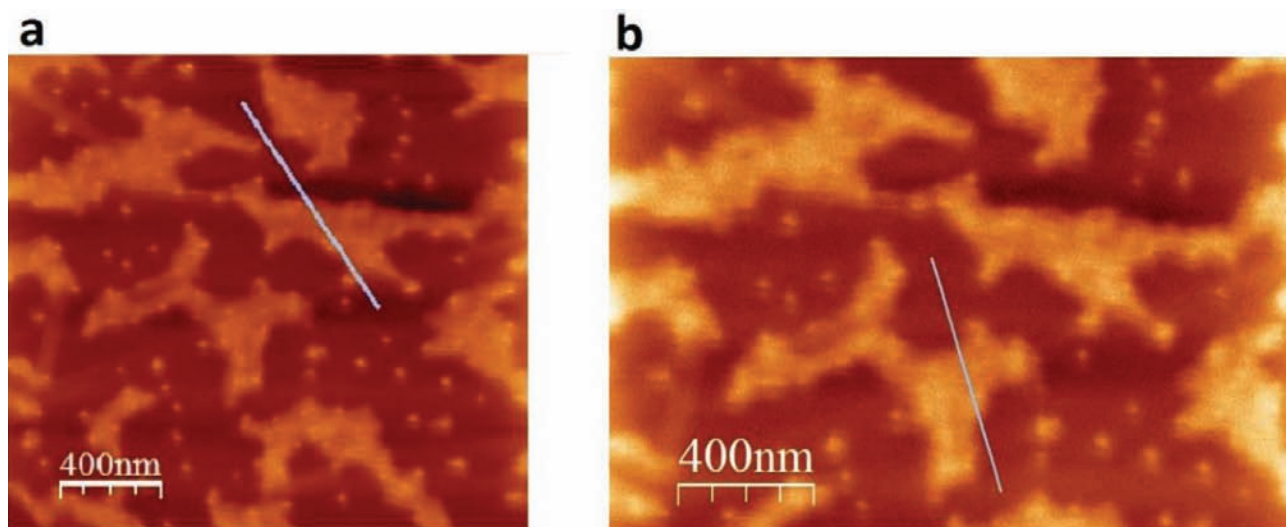
Figure 7. AFM images show where the size measurement was performed. Images are from the sample that was dried and topped up with IPA. a) The blue line in the image shows where the height measurement was performed for one nanoisland. b) The blue line in the image shows where the height measurement was performed for a second nanoisland.

found at about 0.9 ± 0.05 nm. The distinct peaks in both height profile and height distribution imply that the nanoparticles were evenly distributed across the surface and no agglomeration or multilayered structure exists.

Dried nanoparticles were topped up with water, and the AFM images obtained from the resultant nanoparticle solution are presented in Figures 9a and 9b. Defect pits in the AFM images were seen, where the pit structure appears to be multilayered in nature. Some silicon nanoparticles were observed to agglomerate on the thin nanoparticle film. The blue lines on the images show where the nanoparticle height profile measurements were performed. The height investigations of the islands are presented in Figure 10.

The height distribution obtained from Figure 9a is presented in Figure 10a. A weak baseline was measured to be 0.3–0.4 nm. The obstacles to height distribution were explained in the previous section. Therefore, the first layer peak was not clearly observed. The second layer peak was observed at 2.2 nm. The third layer peak was observed at about 3.5 nm and the fourth layer peak at about 4.8 nm. Hence, the height distribution gives a particle size of about 1.3 nm. In the height profile investigations, the deviation in size between the first and second layer was observed to be as described in the previous section. The baseline in the height profile measurement was found to be 0.2 nm and the first layer was observed at 0.8 nm. Thus, the nanoparticle size for the first layer was measured as 0.6 nm. The second and third layers were measured as 2 nm and 3.1 nm, which gives 1.1 nm and 1.2 nm as the measured particle sizes for the second and third layers, respectively. The fourth layer was measured at around 4.2 nm, which gives a measured particle size of 1.2 nm for this layer. In general, the results obtained from the height profile were found to be consistent with the height distribution; in both cases, the nanoparticle size for the upper layers was found to lie between 1.1 and 1.3 nm. The first layer's nanoparticle size was measured as 0.6 nm, which was similar to the data obtained from the previous section for the silicon nanoparticles produced in water (see Table 3 for details).

The size investigation of silicon nanoparticles revealed that the nanoparticle size obtained from the measurements was between 0.6 and 1.3 nm. The AFM images showed that the sizes of nanoparticles in alcohol were similar in every layer. No considerable alteration in the size of nanoparticles related to the layer number could be seen. However, when the silicon nanoparticles were transferred to water, there was a significant size
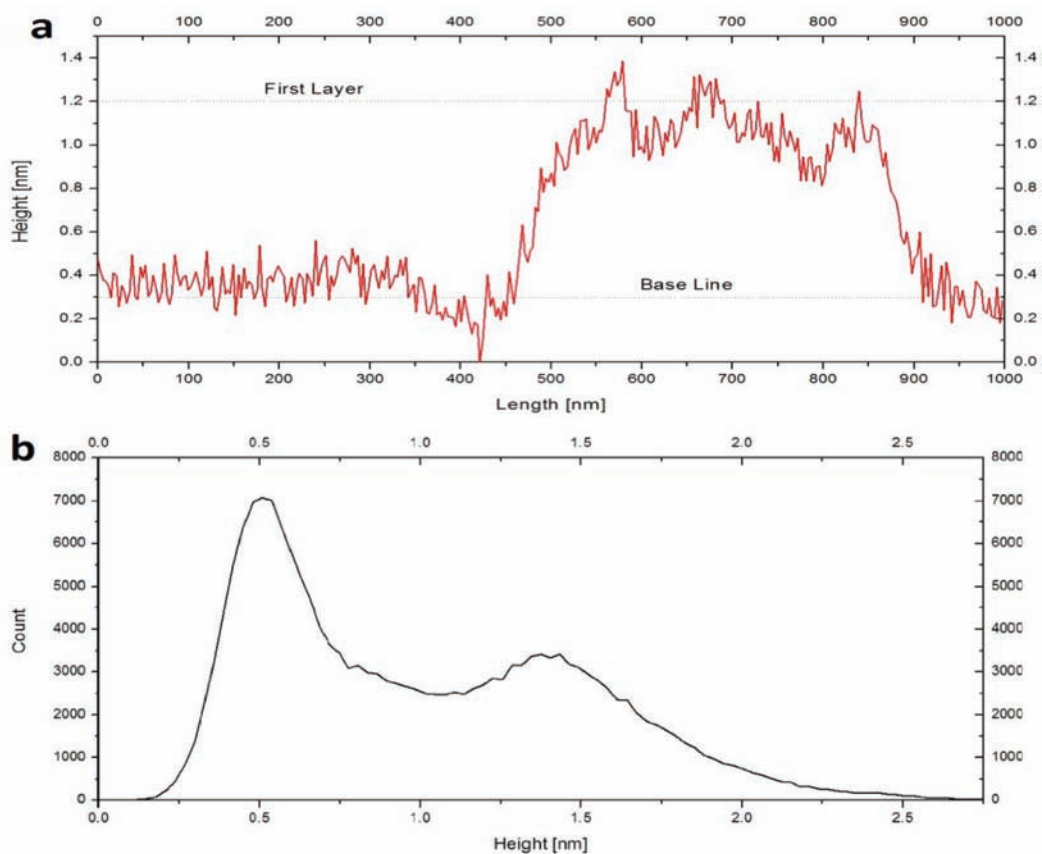
Figure 8. Graphs showing height profiles of the images presented in Figure 7 (IPA sample). a) Graph showing the height profile of the blue line in Figure 7a. Graph showing the height distribution of Figure 7b.
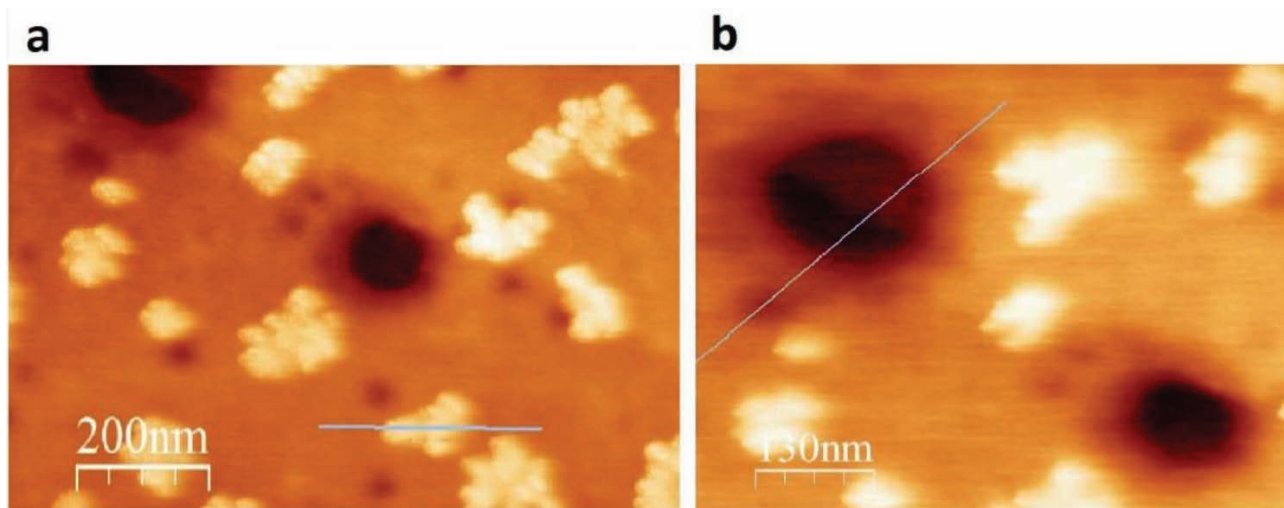

Figure 9. AFM images of multilayered silicon nanoparticles diluted with water. a) The blue line shows the region where the height profile of the agglomerated nanoparticle was taken for an agglomerated nanoisland. b) The blue line shows the region where the height profile was taken for a defect island.
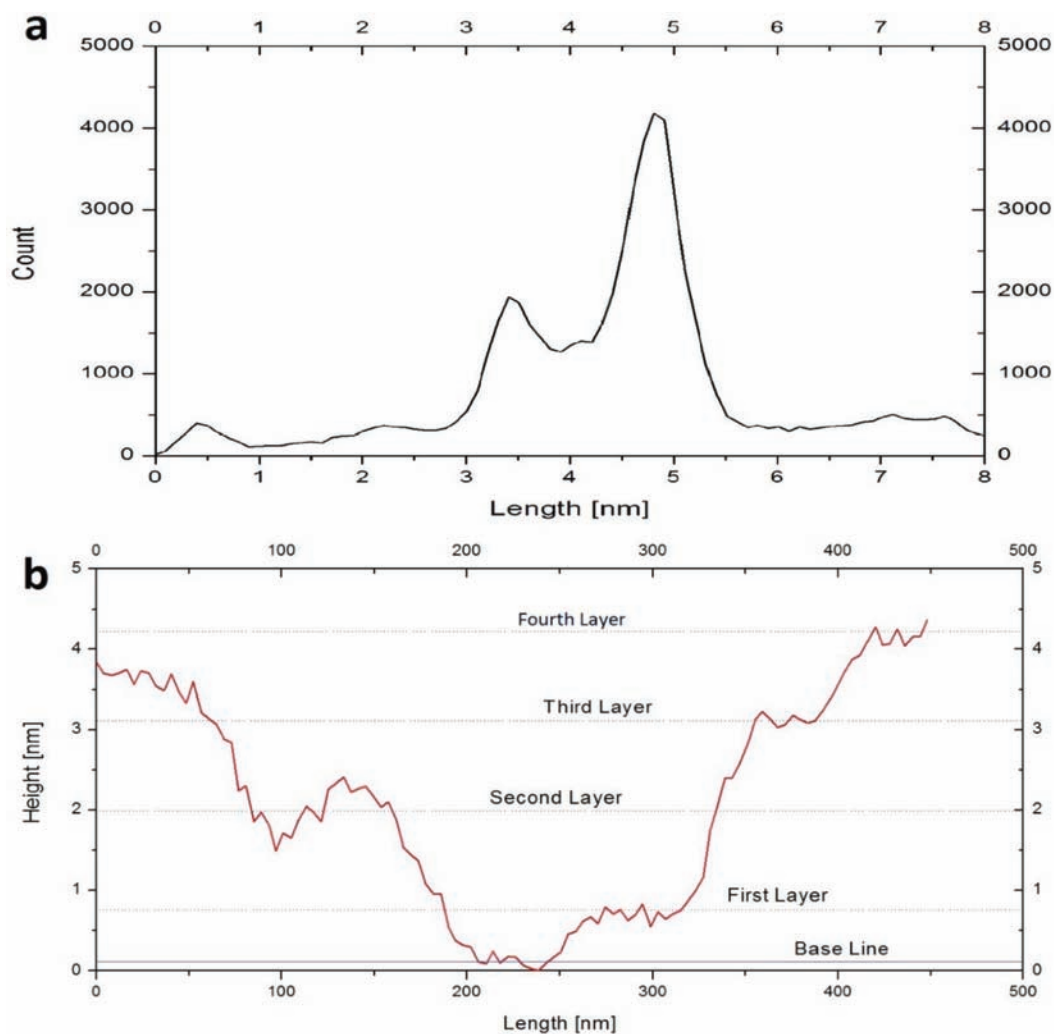
Figure 10. Graphs showing height profiles of the images in the figure (water sample). a) Graph showing the height distribution recorded around the defect island obtained from Figure 9b. b) Graph showing the height profile of the blue line in Figure 9b.

deviation between the first and other layers. As can be seen from the previous section, the investigation of the water containing the silicon nanoparticles produced by the gas aggregation method showed clear height changes between layers as well. It was not surprising to find an alteration of the chemical structure of the nanoparticles in different media. It was suspected that adding water to the silicon nanoparticle solution turned the nanoparticles to highly oxidized silicon nanoparticles or otherwise altered their chemical structure. The alteration in the chemical structure affects the measured size, especially in the first layers.

It was not surprising that chemical change in the structure of the silicon nanoparticles occurred since a size difference was observed for different layers for water containing silicon nanoparticles, whereas no size difference was found for the silicon nanoparticles topped up with alcohol. Yazdanfar also confirmed the chemical alteration of silicon nanoparticles as dependent on solvent type. In the above author's work, nanoparticles that were produced by the liquid jet method were investigated using spectroscopic methods. Yazdanfar found evidence that alterations in the chemical structure for silicon nanoparticles occurred depending on the solvent [35].

4. Conclusion

In this research, noncontact AFM was used to evaluate the size and structure of silicon nanoparticles produced using two different methods in various liquid media. Three main motivations driving this research were the investigation of the size of the silicon nanoparticles produced in water using two different methods: liquid jet, and gas aggregation codeposition with water. We have shown that similar nanoparticle behavior could be observed for particles generated using both techniques. We also used noncontact AFM for the detection of size, where the silicon nanoparticles were found to be smaller than 2 nm. To be more specific, the size of nanoparticles produced by gas aggregation and water codeposition was found to be 0.811 ± 0.07 nm for the nanoparticles in the first layer and 1.35 ± 0.16 nm in the second layer. The change in size for different layers was attributed to surface–particle–tip attractions. The size of nanoparticles produced by liquid jet technique was investigated and solvent dependence was assessed. It was seen that nanoparticles were less than 2 nm. To be more specific, those produced by topping up with ethanol were measured at 1.1 ± 0.15 nm in the first and second layers; no change in size was observed. Silicon nanoparticles topped up with IPA were measured as 0.9 ± 0.05 nm. When the silicon nanoparticles were topped up with water, a change in size between the different layers was observed in a similar manner to the nanoparticles produced using gas aggregation, which here were measured as 0.6 ± 0.1 nm for the first layer and 1.2 ± 0.1 nm for the second and third. This implied a chemical alteration due to changing the solvent, which has also been reported by other researchers, supporting our current observations.

References

[1] Baletto, F.; Ferrando, R. *Rev. Mod. Phys.* **2005**, *77*, 371-423.

[2] Park, T. J.; Papaefthymiou, G. C.; Viescas, A. R.; Moodenbaugh, S. S. *Nano Lett.* **2007**, *7*, 766-772.

[3] Kelly, K. L.; Coronado. E.; Zhao, L. L.; Schatz, G. C. *J. Phys. Chem. B* **2003**, *107*, 668-677.

[4] Fu, H. B.; Yao, J. N. *J. Am. Chem. Soc.* **2001**, *123*, 1434-1439.

[5] Song, J. S.; Choi, S. H.; Seo, D. C.; Oh, M. W.; Yao Cho, T.; Oh, M. H. *J. Cryst. Growth.* **2004**, *264*, 98-103.

[6] Castleman, A. W.; Bowen, K. H. *J. Phys. Chem.* **1996**, *100*, 12911-12944.

[7] Johnston, R. L. *Atomic and Molecular Clusters*; CRC Press: Boca Raton, FL, USA, 2002.

[8] Heiz, U.; Vanolli, F.; Sanchez, A.; Schneider, W. D. *J. Am. Chem. Soc.* **1998**, *120*, 9668-9671.

[9] Moussavizadeh, L.; Von Haeften, K.; Museur, L.; Kanaev, A. V.; Castex, M. C.; Von Pietrowski, R.; Möller, T. *Chem. Phys. Lett.* **1999**, *305*, 327-333.

[10] Gates, B. C. *Chem. Rev.* **1995**, *95*, 511-522.

[11] Ferrando, R.; Jellinek, J.; Johnston, R. L. *Chem. Rev.* **2008**, *108*, 845-910.

[12] Van Orden, A.; Saykally, R. *J. Chem. Rev.* **1998**, *98*, 2313-2358.

[13] Nel, A.; Xia, T.; Mädler, L; Li, N. *Science* **2006**, *311*, 622-627.

[14] Jeng, H. A.; Swanson, J. *J. Environ. Sci. Health. A Tox. Hazard. Subst. Environ. Eng.* **2006**, *41*, 2699-2711.

[15] Karlsson, H. L.; Cronholm, P.; Gustafsson, J.; Moller, L. *Chem. Res. Toxicol.* **2008**, *21*, 1726-1732.

[16] Mader, H.; Li, X.; Saleh, S.; Link, M.; Kele, P.; Wolfbeis, O. S. *Ann. N. Y. Acad. Sci.* **2008**, *1130*, 218-223.

[17] Zhong, Y.; Peng, F.; Wei, X.; Zhou, Y.; Wang, J.; Jiang, X.; Su, Y.; Su, S.; Lee, S. T.; He, Y. *Angew. Chemie Int. Ed.* **2012**, *51*, 8485-8489.

[18] Park, J. H.; Gu, L.; von Maltzahn, G.; Ruoslahti, E.; Bhatia, S. N.; Sailor, M. J; *Nat. Mater.* **2009**, *8*, 331-336.

[19] Mohapatra, S.; Mishra, Y. K; Avasthi, D. K; Kabiraj, D.; Ghatak, J.; Varma, S. *Appl. Phys. Lett.* **2008**, *92*, 103-105.

[20] van Schooneveld, M. M.; Cormode, D. P.; Koole, R.; van Wijngaarden, J. T.; Calcagno, C.; Skajaa, T.; Hilhorst, J.; Hart, D. C.; Fayad, Z. A; Mulder, W. J. et al. *Contrast Media Mol. Imaging.* **2010**, *5*, 231-236.

[21] Santra, S.; Bagwe, R. P.; Dutta, D.; Stanley, J. T.; Walter, G. A.; Tan, W.; Moudgil, B. M.; Mericle, R. A. *Adv. Mater.* **2005**, *17*, 2165-2169.

[22] Santra, S.; Zhang, P.; Wang, K.; Tapec, R.; Tan, W. *Anal. Chem.* **2001**, *73*, 4988-4993.

[23] Rosso-Vasic, M.; Spruijt, E.; Popović, Z.; Overgaag, K.; Van Lagen, B.; Grandidier, B.; Vanmaekelbergh, D.; Domínguez-Gutiérrez, D.; De Cola, L.; Zuilhof, H. *J. Mater. Chem.* **2009**, *19*, 5926-5933.

[24] Li, Z. F.; Ruckenstein, E. *Nano Lett.* **2004**, *4* , 1463-1467.

[25] Erogbogbo, F.; Swihart, M. M. T. *MRS Proc.* **2006**, *958*, 908-958.

[26] Härting, M.; Zhang, J.; Gamota, D. R.; Britton, D. T. *Appl. Phys. Lett.* **2009**, *94*, 193-209.

[27] Bapat, A.; Anderson, C.; Perrey, C. R.; Carter, C. B.; Campbell, S. A.; Kortshagen, U. *Plasma Phys. Control. Fusion.* **2004**, *46*, B97-B109.

[28] Ostraat, M. L.; De Blauwe, J. W; Green, M. L.; Bell, L. D.; Atwater, H. A. R. C. J. *Electrochem. Soc.* **2001**, *148*, G265.

[29] Li, X.; He, Y.; Talukdar, S. S.; Swihart, M. T. *Langmuir* **2003**, *19*, 8490-8496.

[30] Ge, M.; Rong, J.; Fang, X.; Zhang, A.; Lu, Y.; Zhou, C. *Nano Res.* **2013**, *6*, 174-181.

[31] Brune, H. *Surf. Sci. Rep.* **1998**, *31*, 125-229.

[32] Bromann, K.; Brune, H.; Röder, H.; Kern, K. *Phys. Rev. Lett.* **1995**, *75*, 677-680.

[33] Brewer, A.; von Haeften, K. *Appl. Phys. Lett.* **2009**, *94*, 261102.

[34] von Haeften, K.; Binns, C.; Brewer, A.; Crisan, O.; Howes, P. B.; Lowe, M. P.; Sibbley-Allen, C.; Thornton, S. C. *Eur. Phys. J. D* **2009**, *52*, 11-14.

[35] Yazdanfar, H. PhD, University of Leicester, Leicester, UK, 2016.

[36] Von Haeften, K. 338 G Galinis - US Patent App. 14/381, 2015.

[37] Horcas, I.; Fernández, R.; Gómez-Rodríguez, J. M.; Colchero, J.; Gómez-Herrero, J.; Baro, A. M. *Sci. Instrum.* **2007**, *78*, 013705.

[38] Galinis, G.; Torricelli, G.; Akraiam, A.; von Haeften, K. *J. Nanoparticle Res.* **2012**, *14*, 1051-1057.

[39] Bergström, L. *Adv. Colloid Interface Sci.* **1997**, *70*, 125-169.

Table S1. Twenty different height profile measurements for the nanoparticles produced using gas aggregation technique in H_2O.

Baseline	First layer	Second layer	Measured height in the first layer	Measured height in the second layer
0.142	0.754	2.34	0.612	1.586
0.096	0.686	2.3	0.59	1.614
0.4	1.1	2.8	0.7	1.7
0.2	0.8	2.83	0.6	2.03
0.05	0.714	2.1	0.664	1.386
0.16	0.816	2.61	0.656	1.794
0.15	0.95	2.15	0.8	1.2
0.1	0.93	2.39	0.83	1.46
0.3	1.08	2.69	0.78	1.61
0.29	1.03	2.39	0.74	1.36
0.089	0.78	1.98	0.691	1.2
0.44	1.3	3.03	0.86	1.73
0.139	0.842	2.92	0.703	2.078
0.115	0.944	2.44	0.829	1.496
0.101	0.89	2.4405	0.789	1.5505
0.5	1.188	3.144	0.688	1.956
0.165	0.804	2.31	0.639	1.506
0.197	0.844	1.989	0.647	1.145
0.435	1.27	2.83	0.835	1.56
0.238	1.025	2.754	0.787	1.729
Average			0.772 ± 0.08	1.584 ± 0.26